Journal of Solid State Chemistry **160,** 362–367 (2001)
doi:10.1006/jssc.2001.9241, available online at http://www.idealibrary.com on IDEAL®

Magnetic and Crystallographic Properties of $LnCrO_4$ (Ln = Nd, Sm, and Dy)

Keitaro Tezuka and Yukio Hinatsu

Division of Chemistry, Graduate School of Science, Hokkaido University, Sapporo 060-0810, Japan

Received January 12, 2001; in revised form April 26, 2001; accepted May 11, 2001; published online July 16, 2001

Zircon-type compounds $LnCrO_4$ (Ln = Nd, Sm, and Dy) were prepared. Their precise crystal structures at room temperature were determined from X-ray diffraction measurements. These compounds have a tetragonal system with space group $I4_1/amd$. Magnetic susceptibility and specific heat measurements have been performed for all the compounds in the temperature range between 1.8 and 300 K. For $NdCrO_4$, an antiferromagnetic transition was found at 25.2 K. $SmCrO_4$ and $DyCrO_4$ show magnetic transitions at 15.0 and 22.8 K, respectively. In addition, structural phase transitions were observed at 58.5 and 31.2 K, respectively. For $DyCrO_4$, the crystal structure below the transition temperature was determined by low-temperature powder X-ray diffraction measurements to be orthorhombic with space group *Imma*. © 2001 Academic Press

INTRODUCTION

Lanthanide complex oxides $LnXO_4$ (Ln = Lanthanides, X = P, V, and As) with the zircon-type structure have been widely investigated. They show interesting magnetic phenomena at low temperatures (1–8). Their magnetic properties are ascribable to the behavior of Ln^{3+} ions in solids because P^{5+}, V^{5+}, and As^{5+} are diamagnetic.

We have been interested in the mixed-metal oxides containing both lanthanides (4*f* electrons) and transition metals (3*d*, 4*d*, or 5*d* electrons). These oxides adopt a diverse range of structures and show a wide range of electronic properties. In this study, our attention has been paid to the lanthanide chromates $LnCrO_4$. It is reported that $LnCrO_4$ (Ln = Nd–Lu, Y) have a zircon-type structure with space group $I4_1/amd$ (No. 141) (9) and that $LaCrO_4$ and $PrCrO_4$ have a monazite-type structure with space group $P2_1/n$ (No. 14) (10, 11). However, little is known about their electronic properties (12–14). Through their magnetic studies, we can expect to obtain an interesting magnetic phenomenon due to the magnetic interaction between their *d* and *f* electrons.

Here, we have prepared zircon-type compounds $LnCrO_4$ (Ln = Nd, Sm, and Dy) and studied their magnetic and crystallographic properties, through X-ray diffraction, magnetic susceptibility, and specific heat measurements.

EXPERIMENTAL

As starting materials, Ln_2O_3 (Ln = Nd, Sm, and Dy) and $Cr(NO_3)_3 \cdot 9H_2O$ were used. These materials were weighed in the correct ratios and dissolved in conc. nitric acid. The nitric solution was evaporated, and the obtained nitrates were heated in an oxygen gas atmosphere at 160°C for 1 h, 200°C for 2 h, and 600°C for 4 h. After cooling, they were ground and heated again in a flow of oxygen gas at 600°C for 4 h.

Powder X-ray diffraction patterns were measured at room temperature and 10 K with Cu$K\alpha$ radiation on a Rigaku RINT2000 diffractometer. The sample was cooled down by using a variable temperature cryostat system CryoMini (Iwatani Industrial Gases Co.).

Magnetic susceptibilities were measured with a SQUID magnetometer (Quantum Design, MPMS model) after zero-field-cooling (ZFC) and field-cooling (FC) processes in the temperature range 1.8–300 K. The external magnetic field applied was 1000 G. The field dependence of the magnetization was measured at 1.8 K by varying the magnetic field strength in the range between −50,000 and 50,000 G.

Specific heat measurements were performed using a relaxation technique by a commercial specific heat measuring system (Quantum Design, PPMS) in the temperature range 1.8–300 K. The sample in the form of pellets was mounted on a thin alumina plate with apiezon for better thermal contact.

RESULTS AND DISCUSSION

Crystal Structures

All the samples prepared in this study $LnCrO_4$ (Ln = Nd, Sm, and Dy) crystallize in single phases. Their X-ray diffraction profiles at room temperature are shown in Fig. 1 and they are indexed with a tetragonal unit cell, space group $I4_1/amd$ (No. 141), indicating that these compounds have

0022-4596/01 $35.00

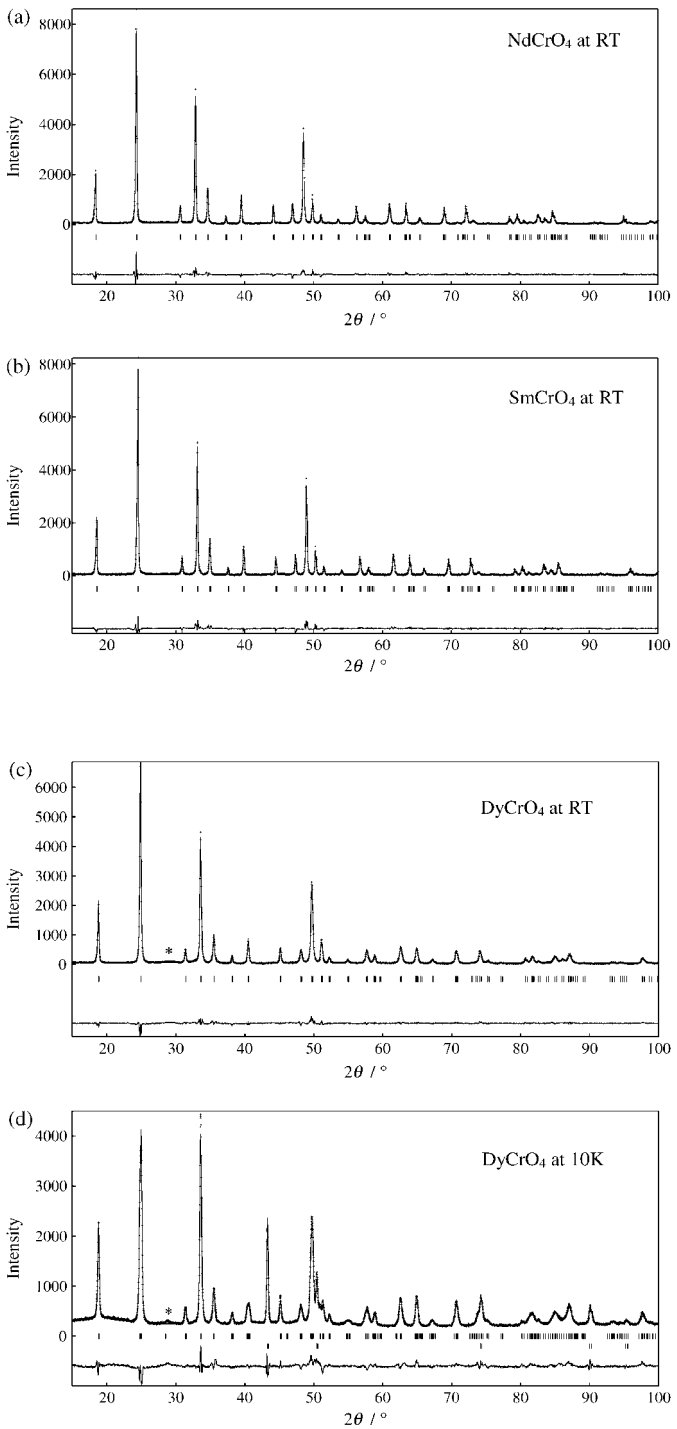

FIG. 1. Powder X-ray diffraction pattern fitting for LnCrO$_4$: (a) NdCrO$_4$ at room temperature, (b) SmCrO$_4$ at room temperature, (c) DyCrO$_4$ at room temperature, and (d) DyCrO$_4$ at 10 K. The calculated and observed patterns are shown on the top solid line and the markers above the peaks, respectively. The vertical marks in the middle show positions calculated for Bragg reflections. The lower trace is a plot of the difference between calculated and observed intensities. For (c) and (d), very broad peaks indicated by the asterisks (*) are identified as Dy_2O_3. The second vertical marks in (d) show the positions calculated for the Cu metal of the sample folder.

TABLE 1
Crystal Structures for LnCrO$_4$ (Ln = Nd, Sm, and Dy)

	NdCrO$_4$	SmCrO$_4$	DyCrO$_4$
a (Å)	7.3118(2)	7.2507(2)	7.1397(3)
c (Å)	6.4002(2)	6.3517(2)	6.2700(2)
y (O)	0.172(1)	0.175(1)	0.185(1)
z (O)	0.337(1)	0.336(1)	0.328(1)
B (Ln) (Å^2)	0.23	0.32	0.29
B (Cr) (Å^2)	0.33	0.41	0.44
B (O) (Å^2)	0.93	0.98	1.04
R_{wp} (%)	12.08	13.98	12.25
R_I (%)	2.84	4.31	5.79
R_F (%)	1.74	2.47	2.87
R_e (%)	7.85	8.17	8.10

Note. Ln, Cr, and O atoms occupy the 4a (0, 0, 0), 4b (0, 0, $\frac{1}{2}$), and 16h (0, y, z) of space group $I4_1/amd$ (No. 141), respectively.

a zircon-type structure. The structural refinements were performed by means of the Rietveld method using the program RIETAN (15). The results (lattice parameters and atomic positions) are shown in Table 1. Some selected bond lengths and angles are listed in Table 2. Figure 2 shows its crystal structure. In these LnCrO$_4$ compounds, the lanthanide ions are eight-coordinated by oxygen ions, and the Ln–O distance becomes shorter in the order of Ln = Nd, Sm, and Dy. This trend is easily understandable by considering the ionic radius of Ln^{3+} (16). The chromium ions are four-coordinated by oxygen ions, and the Cr–O distance becomes longer in the order of Ln = Nd, Sm, and Dy. In the crystal, the Cr site has larger space with shrinking of the Ln–O bonds, and as a result, the Cr–O distance becomes longer with increasing the size of the Ln^{3+} ions. It was reported that lanthanide chromates(V) LnCrO$_4$ containing smaller Ln^{3+} ions than Eu^{3+} ions are lanthanide-deficient; i.e., the chemical formulas are actually $Ln_{0.9}CrO_{3.85}$ as determined by chemical analysis (17). The X-ray diffraction profile for the sample with Ln = Dy prepared in this study shows that small amounts of Dy_2O_3 are contained, and the Rietveld analysis indicates that the chemical formula should be expressed as $Dy_{0.9}CrO_{3.85}$. However, in this study, we

TABLE 2
Bond Lengths (Å) and Angles (°) for LnCrO$_4$
(Ln = Nd, Sm, and Dy)

	NdCrO$_4$	SmCrO$_4$	DyCrO$_4$
Ln–O × 4	2.459(6)	2.422(6)	2.303(6)
Ln–O × 4	2.496(6)	2.479(7)	2.446(5)
Cr–O × 4	1.638(5)	1.641(6)	1.703(5)
Ln–O–Ln × 8	107.3(2)	107.7(2)	110.3(2)
Ln–O–Cr × 4	99.4(3)	98.8(3)	96.5(3)
Ln–O–Cr × 4	153.3(3)	153.4(4)	153.2(3)

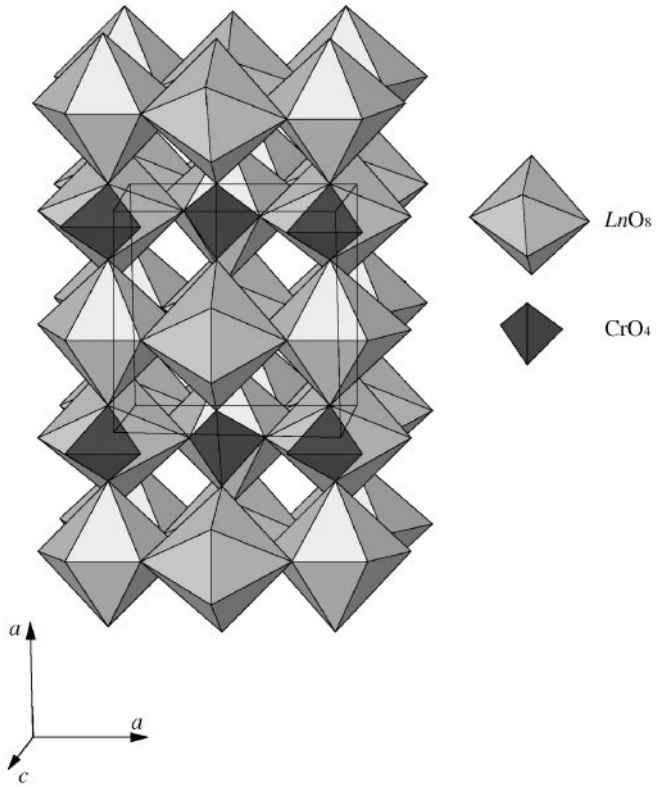

FIG. 2. The crystal structure of $Ln\mathrm{CrO_4}$ (Ln = Nd, Sm, and Dy).

compare the change in magnetic properties of $Ln\mathrm{CrO_4}$ with the kinds of Ln ions, and therefore we use the formula $Ln\mathrm{CrO_4}$ to describe our samples, even for Ln = Dy. The crystal structures of these compounds at lower temperatures will be discussed later.

Magnetic Properties

$NdCrO_4$. Figure 3 shows the inverse magnetic susceptibility of $\mathrm{NdCrO_4}$ as a function of temperature and the inset shows the temperature dependence of the magnetic susceptibility. A magnetic anomaly has been found at approx. 20 K and below this temperature the difference between the ZFC and FC magnetic susceptibilities has been observed, although no magnetic transition was reported in an earlier work (13). The susceptibility obeys the Curie–Weiss law above 30 K. The effective magnetic moment for $\mathrm{NdCrO_4}$ is experimentally determined to be 4.00 μ_B, which is close to the value reported earlier (4.06 μ_B) (13). The theoretical magnetic moment for $\mathrm{NdCrO_4}$ μ_{cal} is calculated by using

$$\mu_{cal}^2 = \mu(\mathrm{Nd}^{3+})^2 + \mu(\mathrm{Cr}^{5+})^2. \qquad [1]$$

Since the effective magnetic moments for Nd^{3+} and Cr^{5+} ions are 3.62 and 1.73 μ_B, respectively, the μ_{cal} is calculated to be 4.01 μ_B, which agrees very well with the experimental

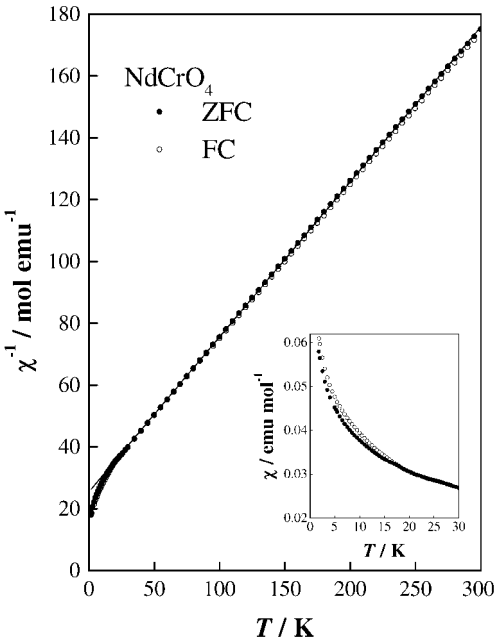

FIG. 3. Temperature dependence of inverse magnetic susceptibilities for $\mathrm{NdCrO_4}$. A solid line represents the Curie–Weiss fitting. The inset shows the magnetic susceptibilities as a function of temperature.

result. The Weiss constant was determined to be a negative value, −51.2 K, which implies that there exists an antiferromagnetic interaction. This value is near to the value reported earlier (−45.5 K) (13).

In order to investigate the anomaly found at approx. 20 K in detail, specific heat measurements were performed. Figure 4 shows the variation of specific heat as a function of

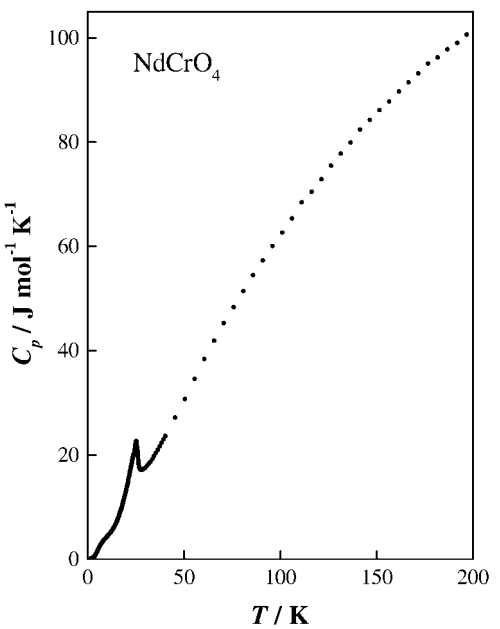

FIG. 4. Specific heat C_p of $\mathrm{NdCrO_4}$ as a function of temperature.

temperature. The λ-type anomaly (which means the existence of magnetic transition) has been found at 25.2 K, which corresponds to the anomaly found in the susceptibility vs temperature curve. A large paramagnetic moment of Nd^{3+} makes the magnetic ordering of Cr^{5+} ions unclear in the susceptibility vs temperature curve. Another specific heat anomaly has been observed at approx. 8 K.

To calculate the magnetic contribution to the specific heat, we subtract the electronic and lattice contributions from the total specific heat. It is known that the electronic and lattice contributions to the specific heat are proportional to the temperature and three powers of temperature, respectively. We evaluate the components of the electronic and lattice contributions by fitting the observed specific heat to the function $f(T) = a \times T + b \times T^2 + c \times T^3$ in the temperature ranges $2.2 < T < 2.8$ K and $60 < T < 70$ K, where little influence of the magnetic transition is expected. Figure 5 shows the magnetic specific heat C_m of $NdCrO_4$ divided by temperature as a function of temperature. A Schottky-type anomaly has been found at 7.9 K.

The crystal field with the point symmetry $\bar{4}m2$ splits the $^4I_{9/2}$ multiplet of paramagnetic Nd^{3+} ion into five Kramers doublets, the energy gap between the ground state doublet and the first excited one being approx. 150 K (5). Thus, at low temperatures, only the lowest doublet ($J = \pm\frac{1}{2}$) is appreciably populated. The magnetic field by the magnetically ordered Cr moments causes the Zeeman splitting of the lowest doublet state of the Nd, and the energy splitting brings about a Schottky-type anomaly. We consider a level of degeneracy g_1, which is Δ in energy above a level of degeneracy g_0. For this two-level system, the Schottky specific heat C_S is given by

$$C_S = \frac{R(\Delta/kT)^2(g_0/g_1)\exp(\Delta/kT)}{[1 + (g_0/g_1)\exp(\Delta/kT)]^2}. \qquad [2]$$

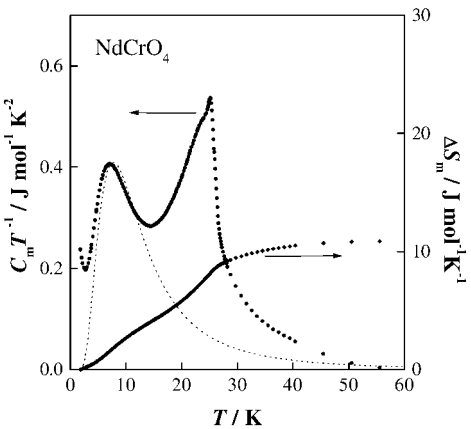

FIG. 5. The magnetic specific heat C_m of $NdCrO_4$ divided by temperature as a function of temperature. The dashed line represents the contribution of a Schottky anomaly of Nd. The lozenge marks (◆) represent the magnetic contribution of the entropy ΔS_m (right ordinate) as a function of temperature.

In this case, the ratio g_0/g_1 is expected to be 1 and the calculated values for the energy gap $\Delta = 25$ K are shown by the dashed line in Fig. 5. Calculation results are in good agreement with the experimental data. In the case of the ratio $g_0/g_1 = 1$, the entropy change due to the Schottky-type anomaly ΔS_S is calculated to be R ln 2 (R is a gas constant) from Eq. [2]. The magnetic contribution of the entropy change ΔS_m is the sum of the entropy change due to the Schottky-type anomaly ΔS_S and the entropy change due to the magnetic transition ΔS_t. Therefore, by subtracting ΔS_S from ΔS_m, the ΔS_t is obtained to be 5.12 J mol^{-1} K^{-1}, which is close to $R \ln(2S + 1) = R \ln 2 = 5.76$ J mol^{-1} K^{-1}, indicating that only two energy levels are involved in the process of magnetic ordering of Cr; i.e., the ground state of Cr is a doublet. The abrupt growth of C_m/T with decreasing temperature below 2.5 K, which is probably due to incorrect estimation of the electronic and lattice contributions to the total specific heat, has been observed.

$SmCrO_4$. Figure 6 shows the temperature dependence of the inverse magnetic susceptibility for $SmCrO_4$. A magnetic transition has been observed at 15.0 K, which agrees with the previous report (13). The divergence between the ZFC and FC magnetic susceptibilities is found below this temperature. In this experiment, another magnetic anomaly has been observed at approx. 60 K as shown in Fig. 6. Specific heat measurements show an anomaly at nearly the same temperature, 58.5 K (see Fig. 7). We consider that this anomaly should correspond to the structural phase transition in a manner similar to the case of $DyCrO_4$ to be

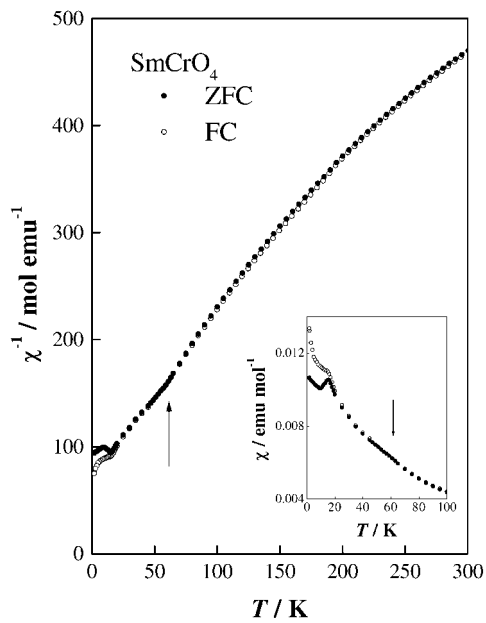

FIG. 6. Temperature dependence of reciprocal magnetic susceptibilities for $SmCrO_4$. The inset shows the magnetic susceptibility vs temperature curve in a lower temperature region.

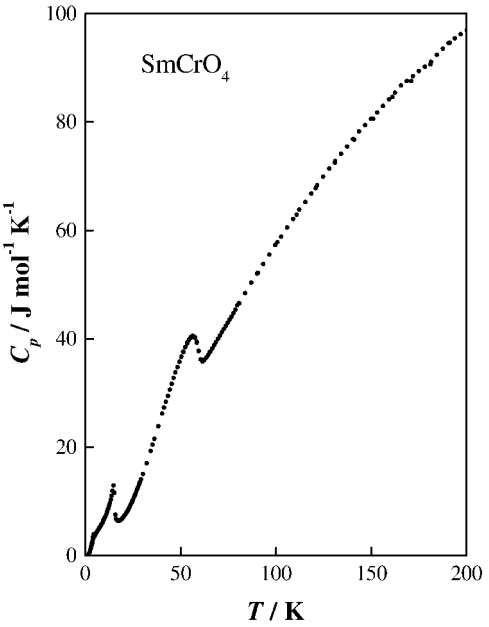

FIG. 7. Temperature dependence of specific heat C_p for $SmCrO_4$.

discussed later, because the Debye temperature seems to change above and below the transition temperature. We will perform low-temperature X-ray diffraction measurements to clarify this transition. A clear λ-type specific heat anomaly has been observed at 15.0 K, which is consistent with the susceptibility measurements.

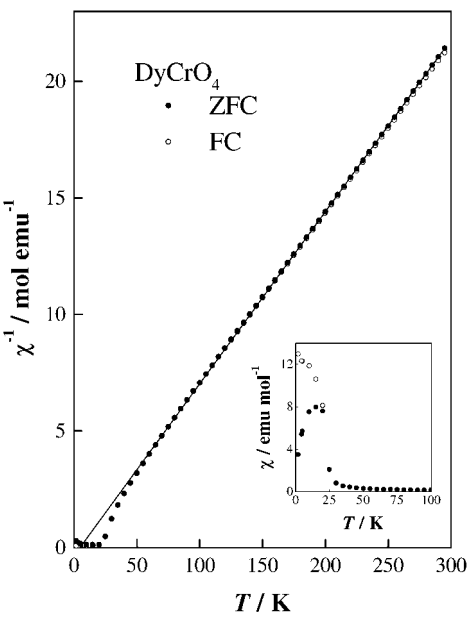

FIG. 8. Temperature dependence of inverse magnetic susceptibility for $DyCrO_4$. The solid line represents the Curie–Weiss fitting. The inset shows the detailed magnetic susceptibility vs temperature curve at lower temperatures.

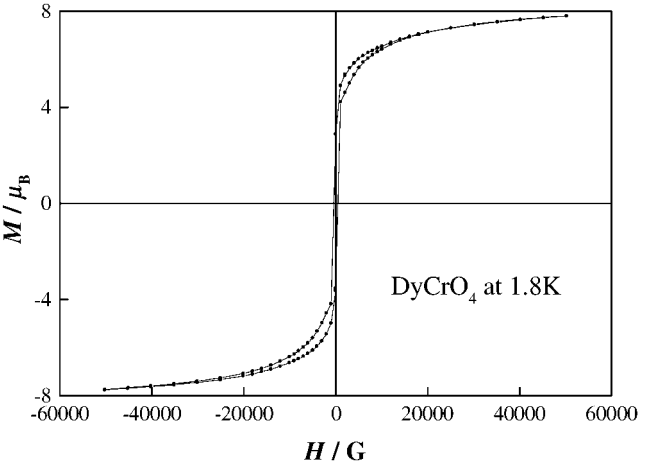

FIG. 9. Magnetic hysteresis curve for $DyCrO_4$ at 1.8 K.

$DyCrO_4$. Figure 8 shows the temperature dependence of the inverse magnetic susceptibility for $DyCrO_4$. A ferromagnetic transition is observed at 23.0 K, which agrees with the previous reports (14, 18). The magnetization measurements have confirmed that magnetic hysteresis exists below this magnetic transition temperature (see Fig. 9). The susceptibility obeys the Curie–Weiss law above 50 K. The effective magnetic moment is determined to be 10.33 μ_B, which agrees well with the calculated moment for $DyCrO_4$ (10.77 μ_B). The Weiss constant is determined to be 7.72 K, indicating the existence of ferromagnetic interactions.

Figure 10 shows the temperature dependence of the specific heat of $DyCrO_4$. A λ-type anomaly has been observed at

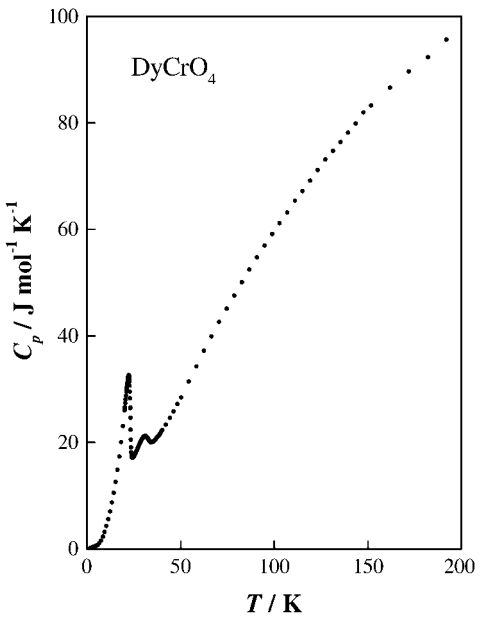

FIG. 10. Temperature dependence of specific heat C_p for $DyCrO_4$.

TABLE 3
Crystal Structure for $DyCrO_4$ at 10 K

Space group *Imma* (No. 74)
$a = 7.173(6)$ Å, $b = 7.114(6)$ Å, $c = 6.268(5)$ Å
$R_{wp} = 7.21\%$, $R_I = 6.45\%$, $R_F = 3.08\%$, $R_e = 5.17\%$

	x	y	z	B (Å^2)
Dy	0	$\frac{1}{4}$	$\frac{7}{8}$	0.09
Cr	0	$\frac{1}{4}$	$\frac{3}{8}$	0.43
O1	0	0.446(1)	0.188(2)	0.51
O2	0.805(1)	$\frac{1}{4}$	0.535(2)	0.30

Dy–O1 × 2	2.20(1) Å	Dy–O1–Dy × 4	114.9(6)°
Dy–O1 × 2	2.41(1) Å	Dy–O2–Dy × 4	108.9(5)°
Dy–O2 × 2	2.26(1) Å	Dy–O1–Cr × 2	150.3(7)°
Dy–O2 × 2	2.55(1) Å	Dy–O1–Cr × 2	94.8(4)°
Cr–O1 × 2	1.82(1) Å	Dy–O2–Cr × 2	158.7(8)°
Cr–O2 × 2	1.72(1) Å	Dy–O2–Cr × 2	92.4(5)°

22.8 K, which is consistent with the results of the magnetic susceptibility measurements. Another anomaly from this study has been found at 31.5 K. In order to investigate this anomaly, powder X-ray diffraction measurements were performed below this temperature (at 10 K). The diffraction profile is shown in Fig. 1d, and it is indexed with an orthorhombic unit cell, space group *Imma* (No. 74). That is, a structural phase transition from the tetragonal phase to the orthorhombic one occurs with decreasing temperature. The results of the Rietveld analysis are listed in Table 3. The orthorhombic distortion, referred to the tetragonal cell, takes place along the [100] direction. This type of phase transition is known to occur at 13.8 and 11.2 K for $DyVO_4$ and $DyAsO_4$, respectively, which is explained by the cooperative Jahn–Teller effect (1). The distortion is due to the splitting of the accidental degeneracy of the crystal field levels. Since the lattice parameters for $DyCrO_4$ are close to those for $DyVO_4$ ($a = 7.1434$ Å and $c = 6.313$ Å) (19), their crystal field effects should be comparable between them, and the Jahn–Teller distortion may occur for $DyCrO_4$.

ACKNOWLEDGMENTS

This work was supported by a Grant-in-Aid for Scientific Research on Priority Area "Novel Quantum Phenomena in Transition Metal Oxides-Spin-Charge-Orbital Coupled Systems" No. 12046203 from the Ministry of Education, Science, Sports, and Culture of Japan, and the Research Fellowships of the Japan Society for the Promotion of Science for Young Scientists. Grateful thanks from the authors are due to Professor K. Konno and Mr. Y. Aoki of Hokkaido University for valuable suggestions and discussion.

REFERENCES

1. G. A. Gehring and K. A. Gehring, *Rep. Prog. Phys.* **38,** 5 (1975).
2. H. Saji, T. Yamadaya, and M. Asanuma, *J. Phys. Soc. Jpn.* **28,** 915 (1962).
3. L. Klein, *Int. J. Magn.* **5,** 231 (1973).
4. K. A. Gehring, A. P. Malozemoff, W. Staude and R. N. Tyte, *Solid State Commun.* **9,** 511 (1971).
5. M.-D Guo, A. T. Aldred, and S.-K. Chan, *J. Phys. Chem. Solids* **48,** 229 (1987).
6. H. Suzuki, Y. Masuda, and M. Miyamoto, *J. Phys. Soc. Jpn.* **52,** 250 (1983).
7. P. C. Hansen, M. J. M. Leask, B. M. Wanklyn, Y. Sun, R. L. Cone, and M. M. Abraham, *Phys. Rev. B* **56,** 7918 (1997).
8. A. Kasten, *Z. Phys. B* **38,** 65 (1980).
9. G. Buisson, F. Bertaut, and J. Mareschal, *C. R. Acad. Sci. Paris* **259,** 411 (1964).
10. S. G. Manca and E. J. Baran, *J. Phys. Chem. Chem. Solids* **42,** 923 (1981).
11. R. C. L. Mooney-Slater, *Z. Kristallogr.* **117,** 371 (1962).
12. A. Morales-Sánchez, F. Fernández, and R. Sáez-Puche, *J. Alloys Compd.* **201,** 161 (1993).
13. E. Jiménez, J. Isasi, and R. Sáez-Puche, *J. Alloys Compd.* **312,** 53 (2000).
14. H. Walter, H. G. Kahle, K. Mulder, H. C. Schopper, and H. Schwarz, *Int. J. Magnetism* **5,** 129 (1973).
15. F. Izumi, "The Rietveld Method" (R. A. Young, Ed.), Chap. 13. Oxford Univ. Press, Oxford (1993).
16. R. D. Shannon, *Acta Crystallogr. A* **29,** 751 (1976).
17. Y. Aoki and H. Konno, *J. Mater. Chem.* **11,** 1458 (2001).
18. M. Steiner, H. Dachs, and H. Ott, *Solid State Commun.* **29,** 231 (1979).
19. H. Göbel and G. Will, *Phys. Lett. A* **39,** 79 (1972).